Secondary graphitization kinetics in a gray cast iron

Paulo Henrique Ogata [1]*
Wilson Luiz Guesser [2]†
Hélio Goldenstein [3]

Abstract

This work aims to study the solid state graphite precipitation on a grey cast iron during isothermal martensite tempering treatments at high temperatures, a phenomenon known as "secondary graphitization". Samples austenitized at 900 °C and quenched with He, were heated up to 650 °C and maintained at this temperature on a quenching dilatometer. Reactions during heating and during isothermal maintenance were detected through volumetric changes. Kinetics results were interpreted using Burke and Swindells equations.

Keywords: Secondary graphitization; Tempering of the martensite; Kinetics of graphite formation and grey cast iron.

1 Introduction

Grey cast iron is one of the oldest existing engineering materials and is still currently used in many applications. It presents several unique properties, while being one of the less expensive factory produced structural material. It is a versatile casting alloy, thanks to its high fluidity, low contraction and excellent machinability. Gray cast iron is usually used in applications that require high vibration damping and good heat dissipation, as internal combustion engine blocks, disk and drum brakes, rotors, machine tool frames, etc. The presence of graphite particles originated from the solidification have been shown to be an important strategy for reducing friction during metal/metal sliding, conferring self-lubricating properties to the material.

Secondary graphitization, the nucleation of a large number of small nodules in the solid state, usually during high temperature tempering of a quenched martensite matrix, or alternatively after maintaining a pearlitic microstructure at high temperatures for a long time, is usually considered harmful. Secondary graphitization reduces the yield strength and hardness, as it is associated with complete ferritization of the matrix and the large number of small nodules formed constitute easy nucleation sites for initiating ductile fracture (dimples). Usually seen in quenched and tempered ductile cast iron or graphitic steels, it has also been shown to lower the ductile to brittle transition temperature, allowing the use of critical components in sub-zero temperatures [1,2]. Recently different novel strategies were developed in order to obtain fine dispersions of graphite as a solid lubricant for use in components subjected to metal/metal sliding [3]. This work was inspired on the idea that secondary graphitization could attain similar purpose.

The formation of secondary graphite does not only happens in cast irons. In steels, the formation of graphite can occur when the material is kept for very long periods of time at temperatures close or above 400 °C. The formation of graphite in these cases occurs by a decomposition of cementite to ferrite and graphite. This secondary graphitization can be the cause of failure in creep resistant steels subjected to extended times (years) of service at high temperatures [4]. There are also graphitic steels grades, where the secondary graphitization is part of the normal processing [5-7]. The morphology of graphite in steels is of the nodular or multifaceted type, similar to cast irons.

In order to obtain secondary graphitization in cast iron, the iron is heated to the austenite + graphite field and cooled with high cooling rates, typically quenching in heated oil to avoid possible cracks. Fast cooling delivers instant transformation of the austenite to martensite plates and retained austenite. Subsequent tempering at low temperatures will first precipitate transition carbides, then above 350/400 °C precipitate cementite, decompose the retained austenite and finally recrystallize the martensite. Tempering at even higher temperatures (typically above 600 °C) will cause the dissolution of cementite and precipitation of secondary graphite, as final stage of the tempering treatment.

The secondary nucleation of graphite can be influenced by different factors such as chemical composition of the

[1]Departamento Mecânica: Processos de Soldagem, Faculdade de Tecnologia de Itaquera, FATEC Itaquera, São Paulo, SP, Brasil.
[2]Universidade de Santa Catarina, UDESC, Joinville, Santa Catarina, SC, Brasil.
[3]Laboratório de Transformações de Fases, Departamento de Engenharia Metalúrgica e de Materiais, Escola Politécnica, Universidade de São Paulo, USP, São Paulo, SP, Brasil.
†Posthumous tribute

*Corresponding author: paulo.ogata@fatec.sp.gov.br

cast iron, temperature and time of austenitizing, presence of microstructural defects, as shown by Pimentel [8,9].

The austenitizing temperature and treatment time affect the concentration of carbon in austenite, a fact that influences the morphology of the microstructure and hardness of the martensite after tempering. Askeland et al. [10] studied the effects of austenitizing temperature on a ductile cast iron austenitized for two hours, quenched and then tempered at 677 °C, also for two hours. Austenitizing treatments performed on samples of nodular cast iron at temperatures below 816 °C did not form secondary graphite. Askeland et al. [10] also determined that in order to occur secondary nucleation of graphite, the carbon concentration in martensite needs to be at least 0.35% by weight. The austenitizing treatment soaking time influences the amount of solubilized carbon in austenite (martensite after quenching) and therefore the amount and morphology of the secondary graphite (after tempering treatment). The holding time at the tempering temperature also has an important role: for short tempering treatments the number of secondary graphite nodules per unit area is small, probably because the carbon available to precipitate in the martensitic matrix is limited by the rate of dissolution of the cementite.

This paper describes the secondary graphitization of a lamellar graphite cast iron that has been austenitized and quenched, and finally tempered at temperatures below the eutectoid temperature.

2 Materials and methods

The chemical composition of the grey cast iron is shown in Table 1.

The first step was to characterize the sample in as received condition. The surfaces were prepared using conventional metallographic techniques and characterized by optical electron microscopy (OM). Subsequently, the mechanical properties were evaluated by hardness measurements. Next, in order to find the appropriate austenitizing temperature to the material under study, a thermodynamic simulation was run in order determine the equilibrium phases at different temperatures using the Thermo-Calc® and TCFE database.

Dilatometric experiments were run on a quenching dilatometer Bähr DIL 805A at the Laboratory of Phase Transformations, Department of Metallurgical Engineering, Escola Politécnica da Universidade de São Paulo. The specimens used in the dilatometer had dimensions Ø4 mm × 10 mm.

The complete thermal cycle (austenitizing and tempering) was carried in the dilatometer without opening the chamber, as outlined in Figure 1. Heating was performed under vacuum at a rate of 20 °C/s up to the temperature of 900 °C, which was maintained for 120 sec prior to rapid cooling at a rate of 100 °C/s using helium gas. In the tempering step the samples were heated at a rate of 20 °C/up to 650 °C, the temperature maintained for 5 h before cooling at a rate of 65 °C/s with helium gas.

The hardness of the specimens was determined by the Brinell test. Four indentations were made for each condition. The load used was 187.5 kg with a 2.5 mm ball.

To quantify the number of graphite particles, the hardness and the volume fraction of secondary graphite, samples with dimensions of 9.5 mm × 9.5 mm × 4 mm were subjected to austenitizing treatments in a salt bath at 850 to 900 °C for one hour followed by quenching in oil. The subsequent tempering treatment was conducted at a temperature of 650 °C for 3, 6, 9, 30, 60, 90, 120, 165, 240 to 300 minutes, also on a pit type salt bath furnace. The heat-treated samples were metallographically prepared and characterized by scanning electron microscopy.
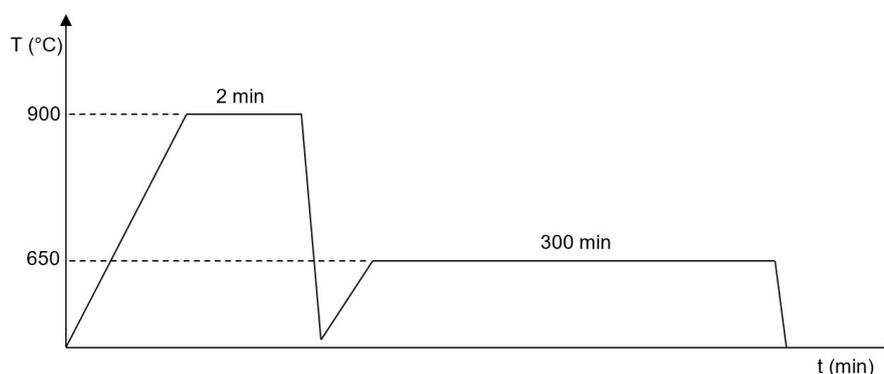

Figure 1. Thermal cycles used in dilatometer test.

Table 1. chemical composition of grey cast iron. (mass percent)

Material	C	Si	Mn	P	S	Cr	Cu	Cr
FOFCZ	3.15	2.8	0.4	<0.04	0.1	<0.03	0.5	<0.03

3 Results and discussion

3.1 As received sample

Cut and polished as received samples were observed metallographically without etch to characterize the solidification graphite morphology and distribution; afterwards nital 2% etch was used to characterize the matrix.

The graphite morphology was not homogeneous, with different regions presenting lamellar and compact graphite forms, types A, B, D, as well as dendrites (Figure 2).

After metallographic etching, dendrite arms proved to be composed of perlite, as shown in Figure 3. In the interdendritic region types A and D flake graphite can be observed along to elongated manganese sulfide inclusions (gray microconstituent).

3.2 Thermo-Calc® simulation

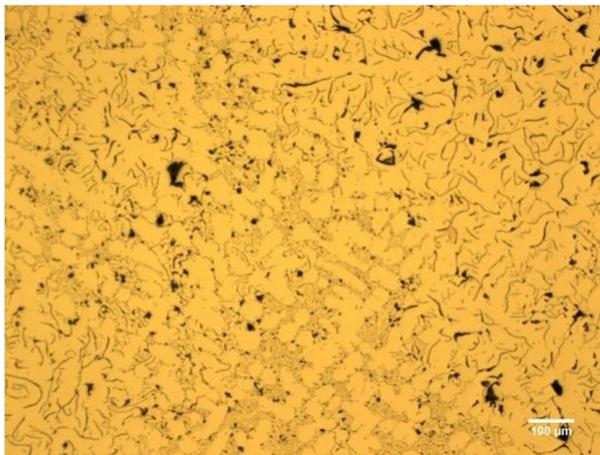As can be seen in Figure 4 at the temperature to 900 °C the equilibrium phases are austenite and graphite.

The relatively low temperature used follows Askeland's reasoning, that lower austenitizing temperatures would result in fine martensite laths that in turn would favor the abundant nucleation of secondary graphite [10]. The author also stated that the most significant factor in the formation of secondary graphite is related to the larger area of interface of martensite laths. However, too low austenitizing temperatures leads to depletion of carbon in austenite, impeding the graphitization reaction.

3.3 Dilatometric test

Figure 5 represents the complete curve of a dilatometric test, comprising the steps of austenitizing, quenching and tempering. The total expansion of the sample was 44 μm but this extension is the cumulative result of all changes inherent to the material, such as martensite transformation, carbon enrichment of the retained austenite, tetragonality loss during the tempering of martensite, carbides formation/dissolution, and finally secondary graphitization. After austenitizing the sample expanded 49 μm, a dilation corresponding to the martensitic transformation, minus the retained austenite.

3.3.1 Step austenitizing

Figure 6 shows the dilation vs temperature results corresponding to the austenitizing and quenching step. The sudden expansion at 207 °C, indicate the beginning of the martensitic transformation event (ie, the Ms temperature).

The micrographs in Figure 7 illustrate the microstructures corresponding to the first two main events seen during the complete dilatometric essay as seen in Figure 5. Figures 7a (optical) and 7b (SEM) correspond to the martensite + retained austenite matrix after the first cooling - event 1.

Figures 7c and 7d shows the tempered martensite matrix - event 2, a sample quenched and reheated at 20 °C.sec^{-1} up to 560 °C, then rapidly cooled with He gas. The white regions were interpreted as retained austenite.

Figure 2. Grey cast iron (as received) without etching.

(a)

(b)

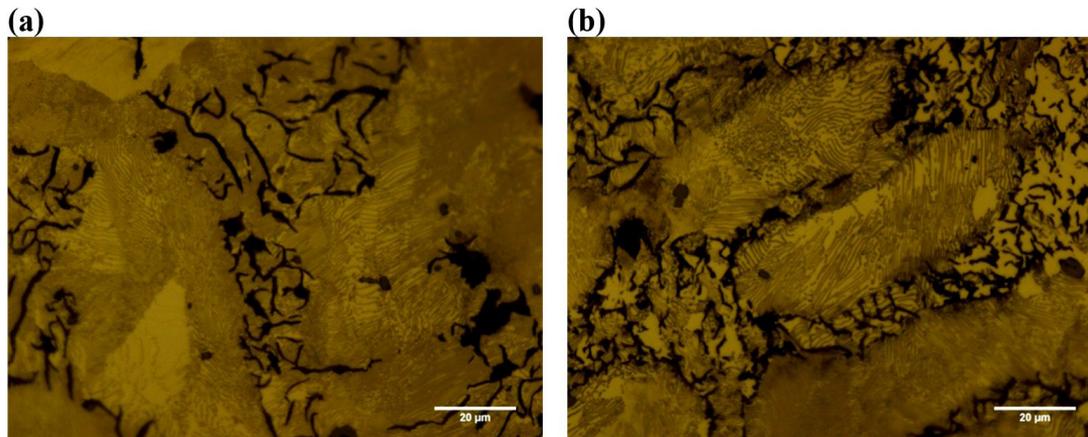**Figure 3.** Microstructure of the grey cast iron (as received) etching (Nital 2 %). (a) Flake graphite; (b) E-type graphite.
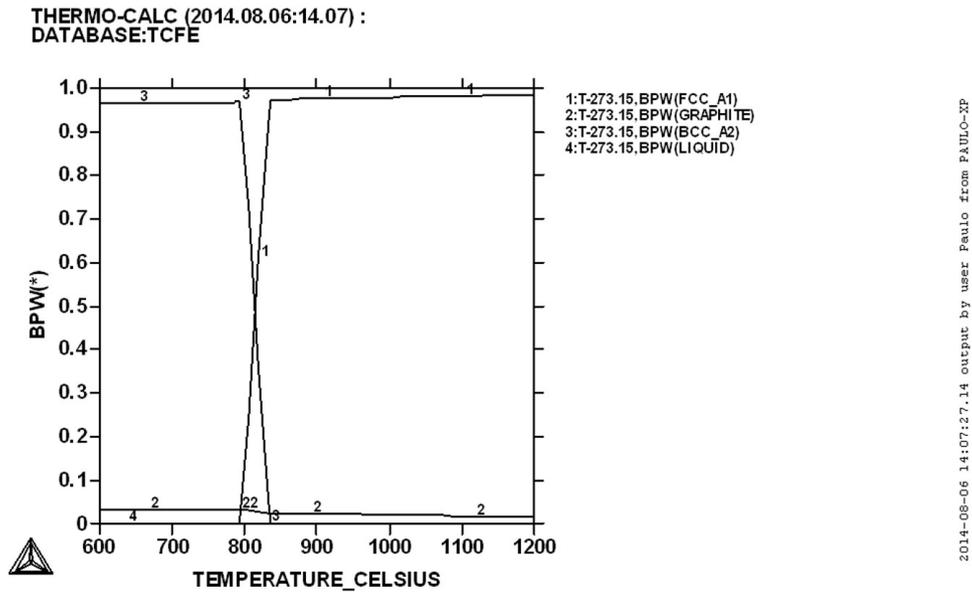
Figure 4. Phases map for the studied grey cast iron, obtained from ThermoCalc.

In bainitic steels and cast irons, Si retards the precipitation of cementite from austenite during the bainitic reaction, allowing the enrichment of carbon in austenite, stabilizing the retained austenite up to room temperature [11]. Similar phenomena occur during tempering of martensite and retained austenite during Quenching and Partition experiments and in ADI, austempered ductile iron [12].

The volumetric fraction of retained austenite decreases during reheating, while the carbon concentration in austenite increase during reheating at 20 °C.sec^{-1}.

In Figure 7d carbon depleted martensite containing precipitated carbides and stabilized austenite blocks are observed, the austenite probably stabilized by carbon partition from the martensite.

The reaction sequence for tempering of martensite in steel proposed by Speich [13] can be adapted to grey cast iron, with the introduction of a fourth tempering stage: reheating at 650 °C results at first in recrystallization of ferrite, cementite precipitation and coarsening but after some time, there is graphite nucleation and growth, at the expense of the temper cementite, which gradually dissolves – event 3.

The resulting microstructure at the end of the isothermal treatment can not be seen in Figure 8, with the presence of manganese sulfide inclusions, a few remaining carbides and secondary spheroidal graphite morphology dispersed in a ferritic matrix.

The kinetics of the reactions arising during tempering was studied using the results obtained by dilatometry. The portions corresponding to isothermal treatment in the expansion versus time curve was separated from the full curve (Figure 5) as shown in Figure 9.

The transformed fraction was determined from the lever rule in dilation versus time curve as described in Marra and Santos [14] article. The kinetic equation was fitted by
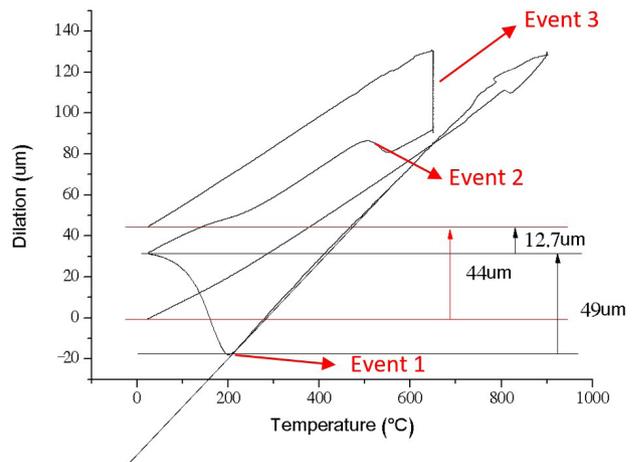

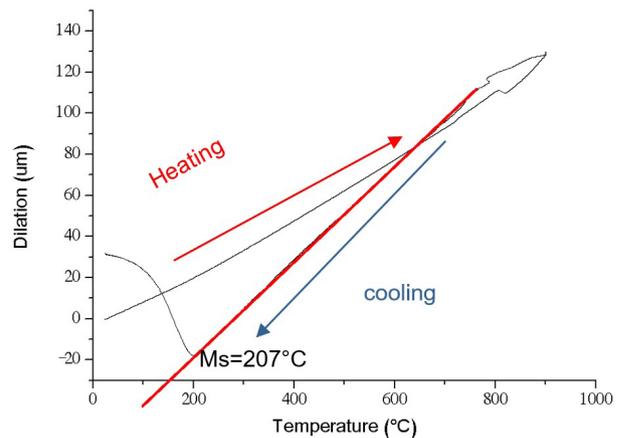**Figure 5.** Complete curve of the grey cast iron obtained in dilatometer test.

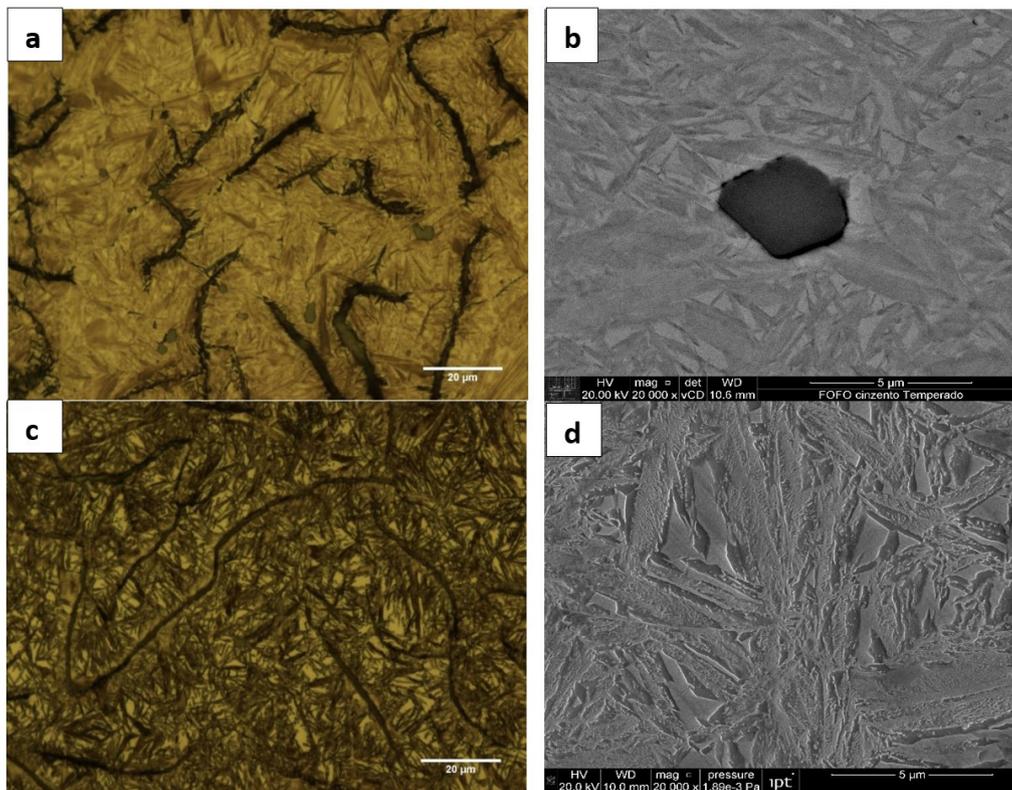**Figure 6.** Dilatometry curve obtained during austenitizing and quenching step

Figure 7. Micrographs (a) and (b) correspond to the quenched sample (event 1); (c) and (d) correspond to the tempered (event 2) interrupted at 560 °C, before the isothermal holding at 650 °C (event 3).
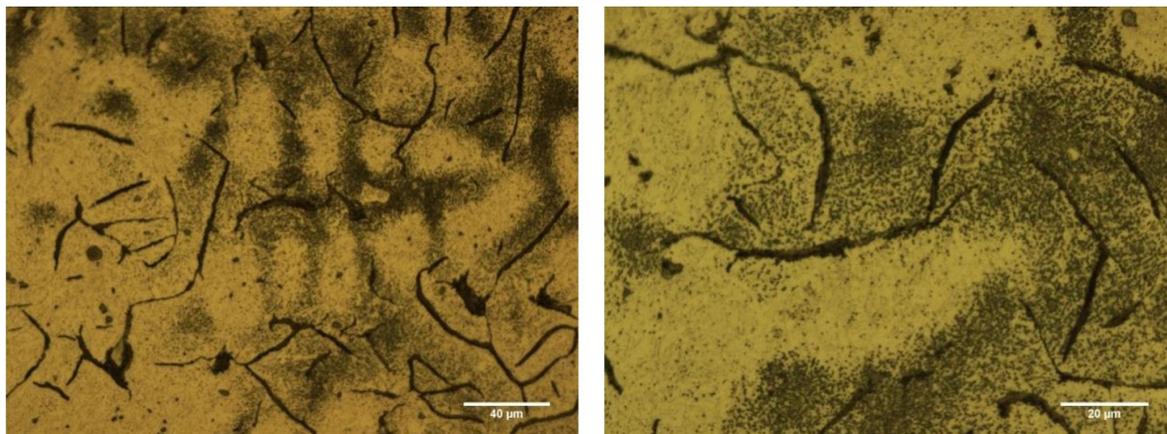

Figure 8. Microstructure of the final isothermal treatments.

Equation 1, as suggested by Burke [15], which is similar to the Johnson-Mehl-Avrami-Kolmogorov (JMAK)) [16] equation. The equation used is distinguished from JMAK by how the constant K is defined. In Equation 1, K has one-time dimension, while in usual manner JMAK representation of the equation, the time constant has dimension n-. Burke reported that from the viewpoint of this situation, activation energy obtained by the dependence of K with temperature cannot be directly compared with the energy obtained when the constant has first-time dimension. Thus, he concludes, it is preferable to avoid this difficulty by using Equation 1.

In Equation 1, Y is the apparent transformed fraction, tending to equilibrium or to the maximum fraction percentage transformed. It is important to realize the distinction between the definition of Y and the volume fraction Vv. Y takes values in the range 0-100%, while the volume fraction of graphite

Ogata et al.

transformed, quantified by quantitative metallography, takes maximum values near 10%.

$$Y = 1 - e^{(-Kt)^n} \tag{1}$$

In the transformed curve apparent fraction (Y) vs. time is obtained by linearizing the experimental data using Equation 2

$$ln\left(ln\frac{1}{1-Y}\right) = (k) + n \cdot ln(t) \tag{2}$$

Dilation results, as shown in Figure 10, were extracted from 0.3 to 0.95 volume apparent fraction (Y), and linearized using Equation 2 (Figure 11). With the choice of starting linearization of the transformed fraction from 0.3 only the growth of graphite is expected to be measured, excluding the spheroidization of temper carbides and the nucleation of graphite phenomena.

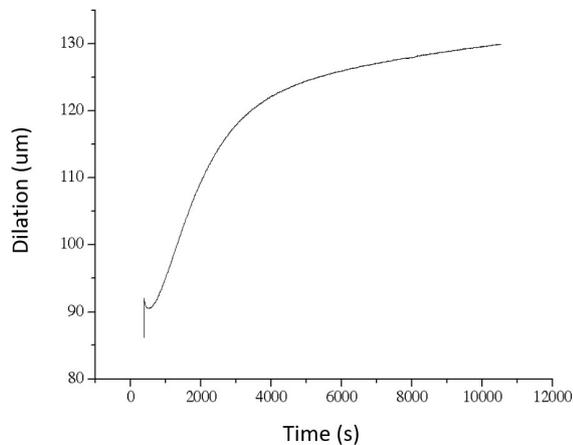From Figure 11 the kinetic coefficients obtained for Equation 2 are K=7.17.10⁻⁴ e n=0.94

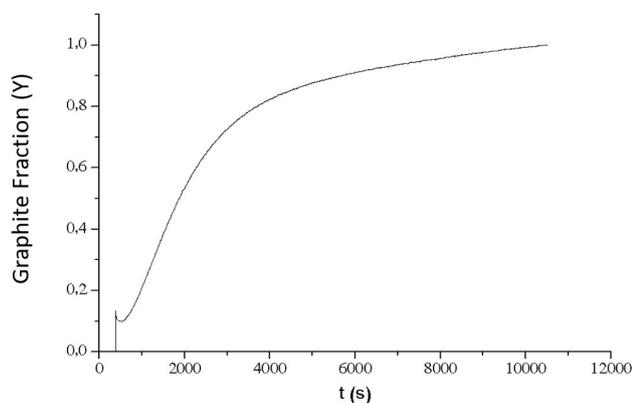**Figure 9.** Dilation curve corresponding only to the isothermal treatments at 650 °C.

Figure 10. Reaction fraction as a function of time for a secondary graphite

According to the literature, values of n = 1 correspond to nucleation at grain boundaries and site saturation, with kinetics controlled by interface or particle growth by diffusion and very low or no nucleation control [16].

3.4 Salt bath heat treatments

The direct determination of the volume fraction and number of graphite nodules isothermally treated in the salt bath was not achieved for the short times of heat treatment, due to the small size of the graphite micro-particles. For longer thermal treatments the particles of graphite become visible by MO and were easier to quantify.

The highest number of nodules were measured after 300 min, with an average 200 nodules per mm². In almost all samples the presence of small manganese sulfides particles, that could easily be confused with graphite nodules, were also observed. In a complementary work [9], the same grey cast iron was austenitized at 900 and 950 °C and tempered at 600 and 650 °C for periods of 2, 5 and 7 hours. For those treatments the nodule counting of secondary graphite reveals a peak of nodules per mm² at about 5 hours, in different conditions of heat treatment. After the formation of secondary graphite nodules, coarsening (Ostwald ripening) of the particles of graphite and/or their dissolution occurs with re-precipitation on the primary graphite. The number of nodules is smaller than the number found for secondary graphitization in ductile cast irons in the literature [1], probably due to smaller amount of C and Si and larger primary graphite interface area, allowing secondary graphite to precipitate also on the boundaries of the primary graphite lamellae.

3.5 Measurements of hardness vs time

The hardness (Figure 12) decreases rapidly after the first three minutes of isothermal treatment (650 °C); remaining relatively constant after 9-60 minutes isothermal treatment and falling again after 90 min.
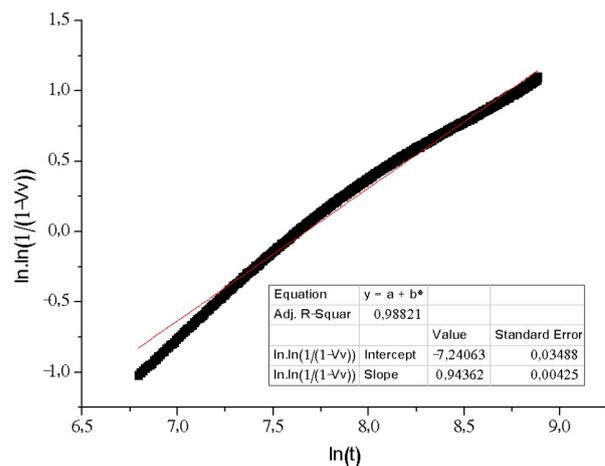

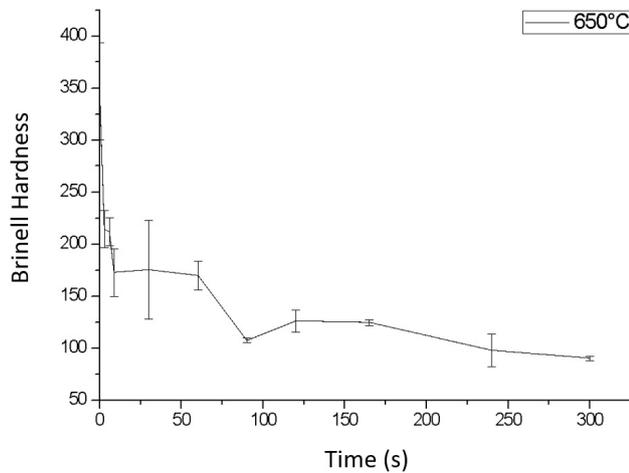**Figure 11.** Linearization curve of the isothermal treatment.

Figure 12. Hardness of the samples in condition of the heat treatment.

4 Conclusions

- Secondary graphitization in cast iron austenitized at 900 °C, quenched and tempered at 650 °C treatments occurs after 5 h;

- The total number of secondary graphite nodules created by the heat treatment was relatively small compared with literature reports for nodular cast iron. This is explained by the lower carbon and silicon and greater competition between precipitation of carbon in the matrix and precipitation at the eutectic lamellae thanks to its large amount of graphite/matrix;

- The hardness decays sharply during the isothermal treatment, falling from about 346 to about 147 HB.

References

1 Vatavuk J, Sinatora A, Goldenstein H, Albertin E, Fuoco R. Efeito da morfologia e do número de partículas de grafita na fratura de ferros fundidos com matriz ferrítica. Metalurgia ABM. 1990;46(386):66-70.

2 Mageza K, Caneia F, Mavhungua S, Banganayia C. Process Improvements of Ferritic Ductile Irons to achieve higher impact properties at subzero temperatures. In: Proceedings of the 2nd Carl Loper Cast Iron Symposium, Latest Advances and Applications of Cast Iron; 2019; Bilbao, Spain. Spain: Azterlan Metallurgy Research Centre; 2019.

3 Klein AN, Binder C, Hammes G, de Mello JDB, Ristow W Jr, Binder R. Self lubricating sintered steels with high mechanical resistance obtained via in situ formation of solid lubricant particles during sintering. In: Proceedings of Euro PM2009 Congress Proceedings; 2009; Copenhagen, Denmark. Chantilly: European Powder Metallurgy Association; 2009. p. 191-196. (vol. 1).

4 Hatakeyama T, Sawada K, Sekido K, Hara T, Kimura K. Graphitization behaviors of creep-ruptured 0.3% carbon steel at 673 to 773 K. ISIJ International. 2021;61(3):993-1001.

5 Iwamoto T, Hoshino T, Matsuzaki A, Amano K. Effects of boron and nitrogen on graphitization and hardenability in 0.53% c steels. ISIJ International. 2002;42(Suppl.):S77-S81.

6 Okamoto A. Graphite formation in high-purity cold-rolled carbon steels. Metallurgical and Materials Transactions. A, Physical Metallurgy and Materials Science. 1989;20:1989.

7 Rounaghi SA, Shayesteh PE, Kiani-Rashid AR. Microstructural study in graphitized hypereutectoid cast and commercial steels. Materials Science and Technology. 2011;27(3):631-636.

8 Pimentel ASO, Guesser WL, Goldenstein H. Formação de grafita secundária em ferro fundido cinzento. In: Proceedings of the 68th ABM International Anual Congress; 2013; São Paulo. São Paulo: ABM; 2013. p. 958-969.

9 Pimentel ASO. Grafitização secundária em ferro fundido cinzento [dissertação]. Joinville: Universidade do Estado de Santa Catarina; 2011.

10 Askeland DR, Farinez F. Factors affecting the formation of secondary graphite in quenched and tempered ductile iron. AFS Transactions. 1979;87:99-106.

11 Caballero F. Dilatometric study of reaustenitisation of high silicon bainitic steels: decomposition of retained austenite. Materials. 2005;46(3):581-586.

12 Nishikawa AS, Miyamoto G, Furuhara T, Tschiptschin AP, Goldenstein H. Phase transformation mechanisms during Quenching and Partitioning of a ductile cast iron. Acta Materialia. 2019;179:1-16.

13 Bhadeshia H, Honeycombe R. Steels: microstructure and properties. 3rd ed. Amsterdam: Butterworth-Heinemann; 2006. 360 p.

14 Marra KM, Santos AA. Método de determinação da cinética de transformação de fases a partir de curvas dilatométricas. In: Anais do Congresso da ABM; 2006; Rio de Janeiro. São Paulo: ABM; 2006.

15 Burke J, Swindells N. The nucleation and growth of graphite during malleabilizing: recent research on cast iron. London: Gordon and Breach Science Publishers; 1968. p. 449-474.

16 Rios PR, Padilha AF. Transformações de fase. São Paulo: Artliber; 2007. 215 p.